Flow in a Turbine Cascade: Part 2—Measurement of Flow Trajectories by Ethylene Detection

J. Moore

B. L. Smith

Department of Mechanical Engineering,
Virginia Polytechnic Institute
and State University,
Blacksburg, Va. 24061

In Part 1 of this paper, measurements of total pressure loss were described at an axial location 40 percent of the axial chord downstream of the trailing edge of a turbine cascade. These results revealed regions of high loss near midspan away from the walls and in the bulk of the flow. In this second part, the origins of fluid in these regions are traced using an ethylene detection technique. Ethylene injection near the blade leading edges and gas sampling downstream and near the blade trailing edges gives information about flow trajectories and mixing through the cascade. Details of the flame ionization detection system used to measure the ethylene concentrations are discussed.

Introduction

In Part 1 [1], we described some measurements of the overall flow development in a linear cascade of turbine blades designed to be geometrically similar to those of Langston et al. [2]. Flow with a relatively thick inlet boundary layer ($\delta^*/\Delta Z \cong 0.023$) on the end walls entered the cascade and a complex three-dimensional flow with large passage vortices developed. Downstream of the cascade, at $x/c = 1.4$, total pressure measurements in the top half of the passage showed a large region of high-loss fluid near midspan. The pitch-averaged losses were lowest at the edge of the endwall boundary layer, due to a low-loss region, and then rose towards midspan. The entropy fluxes (kW/Km^2) normal to the downstream measuring plane were higher at midspan than in the endwall boundary layer. In fact, only 12 percent of the total pressure losses was found in the endwall boundary layer while 58 percent was found in the "high-loss core" near midspan.

In this paper, we attempt to trace the sources of fluid in the high-loss core and in the low-loss region by ethylene injection and detection [3]. We locate fluid from the horseshoe vortices at the blade exit and at the downstream measuring plane, and we infer the flow trajectories of this fluid through the cascade.

Flame Ionization Detection System

A Gowmac model 12-800 flame ionization detector and model 40-700 electrometer were used as the basis of a detection system for ethylene. This system is shown schematically in Fig. 1.

A sample of air and ethylene is drawn isokinetically from the cascade flow field. A steady flow of 55 cc/min of sample is then fed to the flame ionization detector where it is mixed with a hydrogen flow of 20 cc/min. This mixture, with an equivalence ratio of 0.86 (fuel lean), burns as a laminar premixed flame in a surrounding air stream of 250 cc/min. The electrometer applies a potential between the flame holder and a collector downstream. The current flowing between

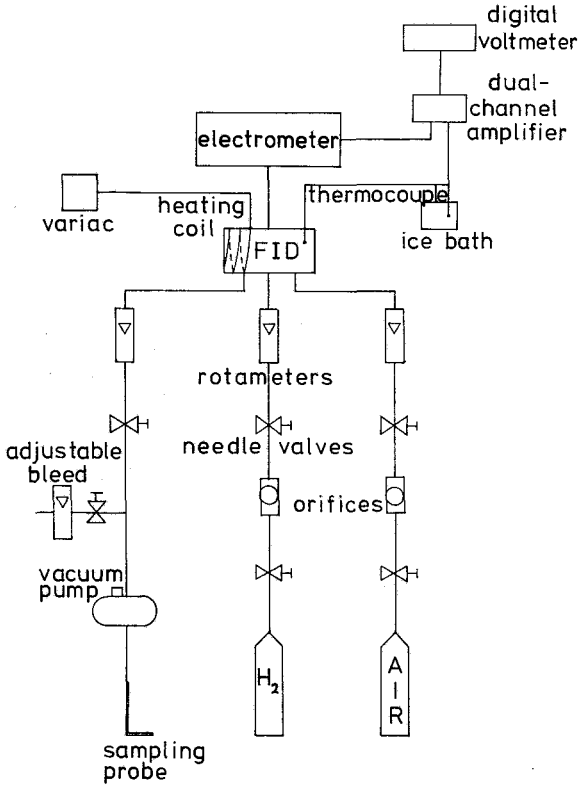

Fig. 1 Schematic of flame-ionization detection system for ethylene

Contributed by the Gas Turbine Division of THE AMERICAN SOCIETY OF MECHANICAL ENGINEERS and presented at the 28th International Gas Turbine Conference and Exhibit, Phoenix, Arizona, March 27-31, 1983. Manuscript received at ASME Headquarters, December 21, 1981. Paper No. 83-GT-69.

Fig. 2 Flow visualization of the limiting streamlines on the bottom wall of the cascade

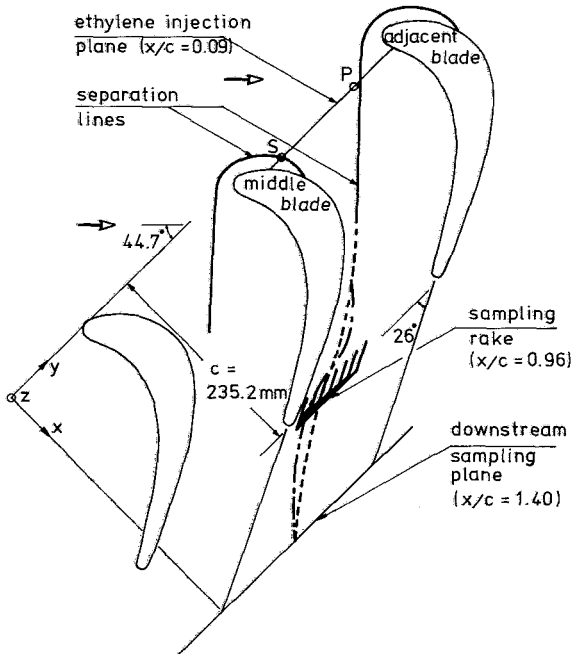

Fig. 3 Top view of test passage showing ethylene injection and sampling planes: 0, injection points for pressure-side (P) and suction-side (S) legs of horseshoe vortex; · · · , likely path of fluid from point P; — - — , likely path of fluid from point S

these two electrodes depends on the conductivity of the burned gas which in turn depends on the ionization of carbon in the sample. The electrometer then gives a millivolt signal proportional to the concentration of ethylene in the sample.

In the present system we further amplified the electrometer output by a factor of about 100 using a differential amplifier with an LM725 operational amplifier. Thus we obtained a signal which could be read directly on a digital voltmeter.

With this flame ionization detector it was important to maintain a very high resistance between the flame holder and the casing. The casing was therefore maintained at a temperature of 120–130° C using a tea-cup heater as an electrical heating coil. This prevented water condensation on the casing walls.

Over the period of the present tests the system response varied from 5 to 6 ppm of ethylene per volt. Care was taken to maintain the sample flow rate constant as the system was more sensitive to changes in this flow than to the hydrogen or air flow rates.

Ethylene injection rates of 150 cc/min were used and during the course of a test the ethylene concentration in the ambient air in the laboratory would vary by the order of 5 ppm. Zero levels were therefore measured by sampling the flow upstream of the cascade.

Tracing Horseshoe Vortex Flow

Figure 2 shows a flow visualization of the limiting streamlines on the endwall of the cascade for the case of the round leading edge which is considered in this paper. The visualization was achieved by rolling a mixture of diesel oil and titanium dioxide onto an aluminum sheet which was taped to the bottom wall; the thin lines on the picture were caused by the edges of the roller. The flow was then turned on for four minutes giving the picture shown. The middle blade of the picture is the middle blade of the five-blade cascade; the

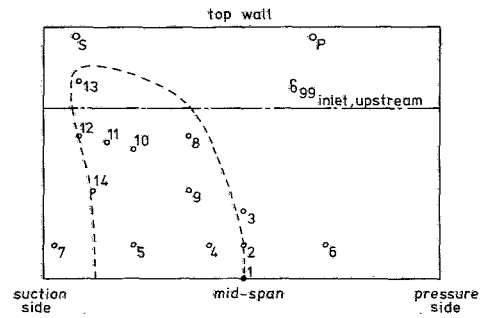

Fig. 4 View of ethylene injection plane (x/c = 0.09) looking upstream: 0, injection points for pressure-side (P) and suction-side (S) legs of horseshoe vortex; 1–14, injection points for tracing low-loss fluid, · · · , estimated locations of fluid with a downstream value of C_{pt} = 0.2

Nomenclature

c = blade axial chord
C_{pt} = total pressure loss coefficient, $\dfrac{p_{t1} - p_t}{\frac{1}{2}\rho U_1^2}$
p_t = total pressure
ppm = parts per million by volume
$\dot{Q}_{C_2H_4}$ = ethylene injection flow rate
U_1 = free stream velocity at inlet
V_n = velocity component normal to downstream measuring plane
x,y,z = cartesian coordinates, Fig. 3
$y_{C_2H_4}$ = mole fraction of ethylene
ΔY = blade pitch
ΔZ = blade span (measured from bottom wall)
δ^* = displacement thickness
ζ = ethylene detection efficiency, equation (1)
ρ = density

Subscript

1 = free stream at inlet

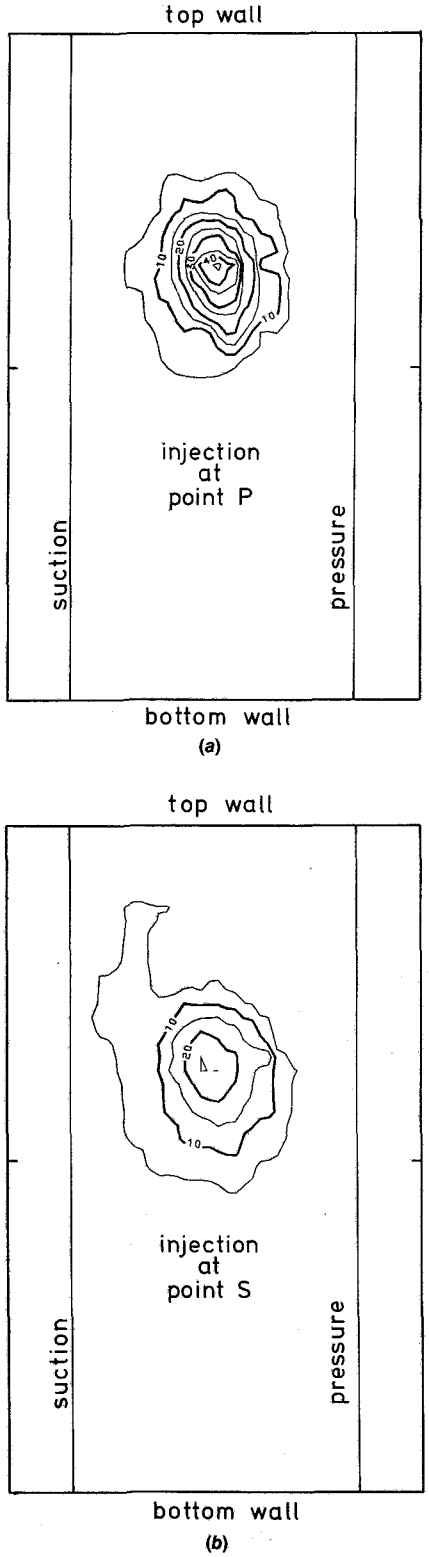

Fig. 5 Ethylene concentration contours at downstream measuring plane (x/c = 1.4). Concentrations in ppm. Contours plotted in cross-sectional plane (see Part 1 [1], Fig. 8) ——— projections downstream of blades in direction of mean camber lines at trailing edges; suction—downstream of middle blade; pressure—downstream of adjacent blade.

present studies were conducted in the flow between this blade and the adjacent blade on the suction side (i.e., the blade in the top right hand corner).

In Fig. 2, the separation of the endwall boundary layer and

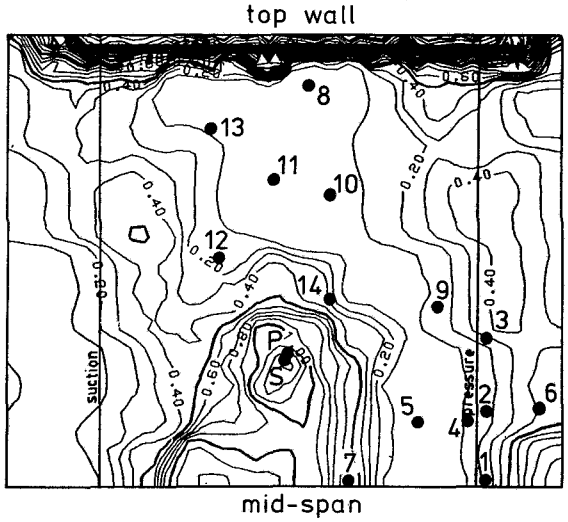

Fig. 6 Contours of total pressure loss coeffcient, C_{pt}, at the downstream measuring plane, x/c = 1.4. Results projected in the cross-sectional plane (see Part 1 [1], Fig 8). •, locations of peak concentrations for injection at the points shown in Fig. 4.

the formation of the horseshoe vortices near the blade leading edges are clearly defined by an accumulation of white titanium dioxide in a line which stretches across the passage to the suction side of the next blade. This almost straight line is associated with the pressure-side leg of the horseshoe vortex which reaches the suction side of the next blade at about midchord, just upstream of the throat. The other leg of the horseshoe vortex stretches around the leading edge and flows down the suction side, where it is clearly seen in the endwall corner region until about the quarter-chord position. At this point it appears to leave the endwall and move onto the suction surface.

The separation lines are also drawn on Fig. 3, which shows a top view of the test passage and sampling planes. The injection plane was at x/c = 0.09 just downstream of the leading edge and the two points, P and S, were chosen for injecting ethylene into the pressure-side and suction-side legs of the horseshoe vortex. The ethylene was injected at a rate of 150 cc/min through 3.1-mm dia tubes located 2.0 percent of the blade span (4.7 mm) from the top wall. Figure 4 shows a cross section of the injection plane viewed from downstream with the injection tubes drawn to scale. The injection was at a distance from the wall of approximately 12 percent of the inlet boundary layer thickness.

Sampling at Downstream Measuring Plane

The flow was sampled isokinetically with a probe of 1.0-mm i.d., which was traversed in the downstream measuring plane. The resulting concentration contours for points P and S are shown in Figs. 5(a) and 5(b), respectively. These plots may be compared with the corresponding contour plot of total pressure loss obtained in Part 1 [1] for the round leading edge, also at x/c = 1.4, and reproduced here in Fig. 6. The locations of the peak concentrations in Figs. 5(a) and 5(b) are marked as P and S in Fig. 6.

Figure 6 shows that the peak concentrations of ethylene from both legs of the horseshoe vortex are found in essentially the same location, at the downstream measuring plane, at a point corresponding very closely with the maximum total pressure loss ($C_{pt} \cong 1.3$) in the high-loss core. The maximum concentration of ethylene from the pressure-side leg of the horseshoe vortex is approximately 45 ppm while the peak from the suction-side leg is 25 ppm. The contours for the pressure-side leg in Fig. 5(a) are quite symmetrical about the peak with a reduction to one-half the peak concentration

Table 1 Distribution of ethylene flow between flow regions at $x/c = 1.4$

	Percentage of measured ethylene	
	Point P	Point S
High-loss core	81%	74%
Blade wake	8%	15%
Low-loss region	9%	8%
Endwall boundary layer	0%	0%

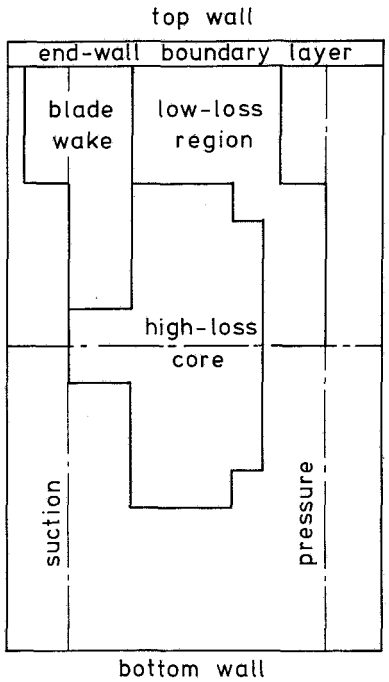

Fig. 7 Areas chosen for numerical integration of ethylene flow rates at $x/c = 1.4$ (see also Fig. 12 of Part 1 [1])

occurring at a radius of about 5 percent of the span. The mixing is somewhat more complete for the suction-side leg and the distribution shows a tail at concentration levels below 10 ppm, as seen in Fig. 5(*b*).

Efficiency of Ethylene Detection

The velocities, V_n, normal to the downstream measuring plane were presented in Part 1 in Fig. 11. These are combined with the measured ethylene mole fractions $y_{C_2H_4}$ to calculate measured ethylene flow rates at the downstream sampling plane. Thus, we define an efficiency of ethylene detection ζ as

$$\zeta = \frac{\int_0^{\Delta Z}\int_0^{\Delta Y} V_n y_{C_2H_4} dydz}{\dot{Q}_{C_2H_4}} \quad (1)$$

where $\dot{Q}_{C_2H_4}$ (= 150 cc/min) is the ethylene injection rate, and ΔY and ΔZ are the blade pitch and span, respectively.

For the two points, P and S, the efficiencies of ethylene detection were 83 and 88 percent, respectively.

Contributions to Ethylene Flow Rate

Comparing the shapes of the ethylene distributions at the downstream plane in Figs. 5(*a*) and 5(*b*), we find a major difference in the maximum concentration and in the tail for point S. The location of the 10 ppm contour is almost identical for both distributions but the maximum concentation for

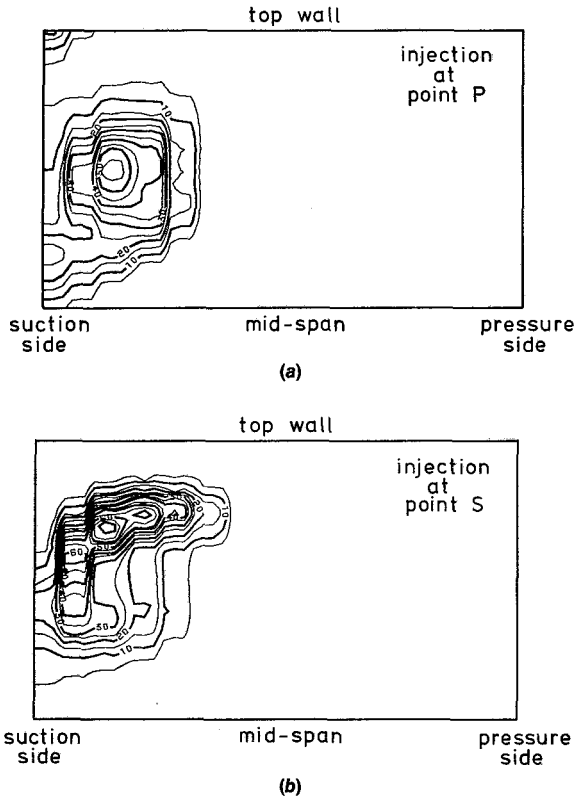

Fig. 8 Ethylene concentration contours near blade exit, $x/c = 0.96$ (concentrations in ppm)

point S is only 25 ppm compared with 45 ppm for point P. This means that less ethylene from point S flows within the high-loss core than from point P. Some of the ethylene from point S is presumably mixed out at concentration levels below 10 ppm in the tail in the blade wake.

In Part 1, we focused attention on four flow regions at the downstream plane. These were the endwall boundary layer, the high-loss core, the blade wake, and the low-loss region, and the corresponding areas of the downstream plane were defined in Fig. 12. Now we can integrate the numerator of equation (1) over these areas to find what fractions of the ethylene from points P and S pass through the high-loss core and what fractions through the other regions. But some of the ethylene measured at the downstream plane was found below midspan and some was found to have crossed the line projected downstream of the trailing edge of the middle blade. The areas for integration were therefore chosen to correspond with the areas shown in Fig. 12 of Part 1 but were modified to include these outside areas as shown in Fig. 7. The results are presented in Table 1 as percentages of the measured ethylene flow rate at the downstream plane.

The results in Table 1 show that the difference between the flow rates in the high-loss core is actually quite small for the two injection points. The percentage of ethylene from point P passing through the high-loss core is 81 percent compared with 74 percent from point S. The difference of 7 percentage points is made up by the blade wake as expected with 15 percent from point S compared with 8 percent from point P. In both cases, the low-loss region accounts for about 8 percent of the ethylene while the remainder was not found in the endwall boundary layer but in the next flow field on the suction side.

These results show that even in this complex flow the location of the peak concentration gives a good indication of the center of the ethylene distribution.

Sampling Near Trailing Edge

A seven-pronged rake was used for sampling just upstream of the blade exit at $x/c = 0.96$ (corresponding to Plane 9 of Langston et al. [2]). This was constructed using 1.6-mm dia tubing soldered in the configuration shown in Fig. 3. It was traversed vertically in the suction-side half of the passage. Figures 8(*a*) and 8(*b*) show the concentration contours at this plane for injection points P and S, respectively.

The contour shapes are quite different for the two injection points. Figure 8(*a*) shows the ethylene from the pressure-side leg of the horseshoe vortex in a relatively symmetrical distribution about a peak concentration of approximately 55 ppm. There is however a ridge of concentrations in excess of 20 ppm extending towards the suction side near midspan. This whole distribution is quite similar to the smoke trace obtained by Stanitz at al. and presented as Fig. 10 in [4]. There they showed the formation of a passage vortex in a 90 deg rectangular elbow by injecting smoke on the plane wall at the elbow inlet. It appears therefore that fluid from point P is distributed throughout the passage vortex just as the smoke in Stanitz's duct marked his passage vortex.

By contrast, Fig. 8(*b*) shows an entirely different distribution of ethylene. Here there is a band of high concentrations, between 50 and 70 ppm, across the top. If the interpretation of the results in Fig. 9 is that fluid from the pressure-side leg of the horseshoe vortex locates the center of the passage vortex at this plane, then the results in Fig. 8(*b*) indicate that fluid from the suction-side leg of the horseshoe vortex is being convected around the center of the passage vortex. Indeed it is already starting another sweep around the center. This could explain the band of high concentrations. In Fig. 3, we have drawn the likely paths of fluid from points P and S between the measured locations of maximum concentrations. These paths are consistent with the picture of fluid from point S being convected around fluid from point P which marks the passage vortex. In this top view, the path of fluid from point S appears like a sine wave, oscillating about the path of fluid from point P.

Consider the orientation of the rake in Fig. 3. A possible explanation of the band of high concentrations in Fig. 8(*b*) is that the path of fluid from point S actually takes it past several prongs of the rake each of which sees the *same* fluid with the same high concentrations.

Mixing Downstream of Blades

Some of the ethylene injected at point S has already diffused to the location of maximum concentration for point P by the blade exit. In Fig. 8(*b*), we find the concentration at this location is 27 ppm. Let us therefore consider the change along a trajectory following the maximum concentration for point P downstream of the blade. Along this trajectory, the change for ethylene from point S is from 27 to 25 ppm, similar to the change for point P, from 55 to 45 ppm. But along a trajectory around the edge of the passage vortex the concentration of ethylene from point S falls from 70 to less than 25 ppm. It appears that fluid at the edges of the passage vortex can mix out quite rapidly compared with fluid in its core. This explanation is consistent with the flow path of the fluid from point S shown in Fig. 3; this carries fluid from point S close to the blade surface at the trailing edge. It is also partly confirmed by the results of Table 1 where we found that 15 percent of the ethylene from point S mixed out at concentration levels below 10 ppm in the blade wake.

Tracing Fluid in the Low-Loss Region

In Part 1, Fig. 12, we defined a low-loss region based on total pressure measurements at the downstream measuring plane. The total pressure contours are reproduced here in Fig. 6 and the low-loss region is essentially that area with $C_{pt} < 0.2$. As discussed in Part 1, it consists of a large low-loss core near the endwall boundary layer with a thin ridge extending to midspan between the high-loss core and the adjacent blade wake. In this section we attempt to find the sources of this fluid in the ethylene injection plane shown in Fig. 3.

To do this, we injected ethylene through a 2.4-mm dia tube at the 14 locations shown numbered in Fig. 4. We then searched the downstream plane at $x/c = 1.4$ to find the peak concentrations. The locations of these we have marked with the corresponding numbers in Fig. 6. We have also estimated with the dotted line in Fig. 4 the location in the injection plane of fluid with a downstream value of C_{pt} equal to 0.2. Thus we see the source of fluid in the low-loss region. The source of this fluid is found in the suction-side half of the passage at the blade inlet where it accounts for approximately 27 percent of the flow area. This is consistent with the fact that fluid in the low-loss region represents about 36 percent of the mass flow through the cascade.

Conclusions

A high-loss core was observed near midspan at the downstream measuring plane ($x/c = 1.4$) in Part 1. Over 65 percent of the ethylene injected near the blade inlet at locations of horseshoe vortex flow was found downstream within this high-loss core. Flow from the pressure-side and suction-side legs of the horseshoe vortex appeared to be distributed around the location of maximum total pressure loss ($C_{pt} \cong 1.3$) in the high-loss core at the downstream plane.

Fluid from the pressure-side leg of the horseshoe vortex appeared to be distributed throughout the passage vortex at the blade exit. The distribution was similar to the distribution of smoke observed by Stanitz in a passage vortex in a rectangular elbow.

Ethylene injected at the location of the suction-side leg of the horseshoe vortex near the blade inlet was convected around the center of the passage vortex. Fluid at the edges of the passage vortex seemed to mix more rapidly downstream of the trailing edge than fluid near its core.

Fluid with low losses ($C_{pt} < 0.2$) at the downstream plane represented about 36 percent of the mass flow through the cascade. At the blade inlet this flow accounted for approximately 27 percent of the flow area.

Acknowledgment

The authors wish to thank Rolls-Royce Limited, Aero Division for supporting this work under a cooperative agreement with Virginia Polytechnic Institute and State University.

References

1 Moore, J., and Ransmayr, A., "Flow in a Turbine Cascade—Part 1: Losses and Leading-Edge Effects," JOURNAL OF ENGINEERING FOR GAS TURBINES AND POWER, Vol. 106, Apr. 1984, pp. 400-408.

2 Langston, L. S., Nice, M. L., and Hooper, R. M., "Three-Dimensional Flow Within a Turbine Cascade Passage," ASME JOURNAL OF ENGINEERING FOR POWER, Vol. 99, Jan. 1977, pp. 21-28.

3 Denton, J. D., and Usui, S., "Use of a Tracer Gas Technique to Study Mixing in a Low Speed Turbine," ASME Paper No. 81-GT-86.

4 Stanitz, J. D., Osborne, W. M., and Mizisin, J., "An Experimental Investigation of Secondary Flow in an Accelerating, Rectangular Elbow with 90 Deg of Turning," NACA TN 3015, Oct. 1953.